Journal of Computational Neuroscience (2018) 44:393–409
https://doi.org/10.1007/s10827-018-0685-9

The effect of inhibition on the existence of traveling wave solutions for a neural field model of human seizure termination

L. R. González-Ramírez[1] · **M. A. Kramer**[2]

Received: 20 June 2016 / Revised: 27 March 2018 / Accepted: 25 April 2018 / Published online: 24 May 2018

Abstract

In this paper we study the influence of inhibition on an activity-based neural field model consisting of an excitatory population with a linear adaptation term that directly regulates the activity of the excitatory population. Such a model has been used to replicate traveling wave data as observed in high density local field potential recordings (González-Ramírez et al. *PLoS Computational Biology*, *11*(2), e1004065, 2015). In this work, we show that by adding an inhibitory population to this model we can still replicate wave properties as observed in human clinical data preceding seizure termination, but the parameter range over which such waves exist becomes more restricted. This restriction depends on the strength of the inhibition and the timescale at which the inhibition acts. In particular, if inhibition acts on a slower timescale relative to excitation then it is possible to still replicate traveling wave patterns as observed in the clinical data even with a relatively strong effect of inhibition. However, if inhibition acts on the same timescale as the excitation, or faster, then traveling wave patterns with the desired characteristics cease to exist when the inhibition becomes sufficiently strong.

Keywords Epilepsy · Traveling waves · Inhibition · Neural field · Seizure termination

1 Introduction

Neural mass models and neural field models have been used to model the dynamics observed in many different brain phenomena. The main simplification of these type of models is based on the assumption that, since the number of neurons and synaptic interactions that produce macroscopic brain phenomena is large, it is feasible to consider a continuum limit and model mean activities of neuronal populations (Coombes et al. 2014; Bressloff 2012; Ermentrout 1998).

There are many different examples of applications of these models to study spatio-temporal patterns of brain activity in the form of stationary bumps, traveling pulses, spiral waves, and more. Bumps of activity are speculated to emerge during spatial working memory tasks and have been studied through a neural field approach in Fuster and Alexander (1971). Also, the authors in Spencer and Schoner (2006) have developed a dynamic neural field theory of spatial working memory. Neural fields have also been used to better understand the effects of anesthetic agents on the EEG (Foster et al. 2011), EEG rhythms (Liley et al. 2002; Nunez 1995), geometric visual hallucinations (Ermentrout and Cowan 1979; Bressloff et al. 2001), activity processing in the rat whisker-to-barrel system (Pinto et al. 1996), among other applications.

The balance between excitatory and inhibitory interactions as well as other biophysical elements permit the existence of different patterns of brain activity. For example, to study brain phenomena without inhibition, neural field models can be developed with an exclusively excitatory weight distribution (e.g., Bressloff 2014). Such disinhibited networks have been shown to support the existence of traveling fronts and waves of activity (Bressloff 2012). This

Action Editor: Bard Ermentrout

Electronic supplementary material The online version of this article (https://doi.org/10.1007/s10827-018-0685-9) contains supplementary material, which is available to authorized users.

✉ L. R. González-Ramírez
lrgonzalezr@ipn.mx

M. A. Kramer
mak@math.bu.edu

[1] Departamento de Formación Básica Disciplinaria, Unidad Profesional Interdisciplinaria de Ingeniería Campus Hidalgo del Instituto Politécnico Nacional, San Agustín Tlaxiaca, Hidalgo, México

[2] Department of Mathematics and Statistics, Boston University, Boston, MA, USA

approach is motivated by experimental observations *in vitro* in which inhibition is pharmacologically blocked and synchronous activity induced via an electrical stimulus (e.g., Huang et al. 2004; Xiao et al. 2012; Golomb and Amitai 1997). Neural field models that include an inhibitory weight distribution have been used to model binocular rivalry waves in visual cortex (Bressloff and Webber 2011) and, through lateral inhibition, produce different spatio-temporal patterns of activity (Amari 1977; Coombes 2005; Pinto and Ermentrout 2001). In the same way, by considering a neural field consisting of an excitatory subpopulation and a negative feedback-mechanism it is possible to prove the existence of different patterns of activity (Bressloff 2014). In particular, traveling waves of activity can be obtained with the inclusion of some form of synaptic inhibition that is not too strong (Amari 1977) or by a non-specific afferent inhibition regulating the excitatory population (Wilson and Cowan 1973). Also, the addition of an inhomogeneous media and its effect on wave propagation failure has been investigated in Bressloff (2001) and Kilpatrick et al. (2008).

Epilepsy has been described as a dynamical disease (Milton and Jung 2003), with characteristic spatio-temporal patterns observed during *in vivo* and *in vitro* recordings in the form of propagation of activity and traveling waves (Milton and Jung 2003; Pinto et al. 2005; Lee et al. 2006; González-Ramírez et al. 2015). Different models have been developed to study epilepsy, including neural mass models with both excitatory and inhibitory populations (Toubol et al. 2013) and continuum or neural field models with interacting excitatory and inhibitory subpopulations (Shusterman and Troy 2008; Jirsa and Haken 1996; Liley et al. 2002; Nunez 1995; Robinson et al. 2001; Bojak et al. 2004; Bojak and Liley 2005; Steyn-Ross et al. 1999; Liley and Bojak 2005; Kramer et al. 2005). In González-Ramírez et al. (2015), the authors used a neural field model consisting of a single activity-based excitatory population and an adaptation term to mimic traveling waves as observed in high density local field potential (LFP) recordings during seizure termination. They obtained parameters ranges for wave propagation in the model with quantitative features consistent with the observed waves. An important assumption of this model was that, approaching seizure termination, the interneurons have inactivated and thus permit the presence of simple dynamics including traveling waves.

In this work, we analyze the conditions that ensure the existence of traveling waves of the model used in González-Ramírez et al. (2015) after considering the inclusion of an inhibitory population. In doing so, we continue to require that the wave propagation in the model remain consistent with features of the traveling wave activity observed preceding seizure termination in the human clinical data described in González-Ramírez et al. (2015). We derive an analytical solution to the model with inhibition, and upon examining different possibilities for the timescale of the inhibitory population we conclude that the addition of an inhibitory population limits the parameter ranges that support wave propagation. In particular, we show that inhibition acting at a slow time scale still permits the existence of waves with the desired characteristics of the *in vivo* data. If inhibition acts on a faster timescale, then increasing the strength of this inhibition restricts the existence of waves with features consistent with the clinical data.

1.1 Model for cortical wave propagation without inhibition

We base our study on the clinical data analysis and model described in González-Ramírez et al. (2015). For this, we briefly review the most important results.

$$\begin{aligned}\frac{du}{dt}(x,t) &= -\alpha u(x,t) + \alpha H\left(\int_{-\infty}^{\infty}\frac{1}{2\sigma}e^{\frac{-|x-y|}{\sigma}}u(x)dy\right.\\ &\quad\left.+P(x,t)-k\right)-\alpha\beta_0 q(x,t)\\ \frac{dq}{dt}(x,t) &= \delta u(x,t)-\delta q(x,t)\end{aligned} \tag{1}$$

Model (1) has been used to replicate important wave features as observed in human clinical data. For a detailed description of the model, see González-Ramírez et al. (2015). The model consists of two variables: $u(x,t)$ represents the neural activity and $q(x,t)$ represents the adaptation at position x and time t. The dynamics of $u(x,t)$ consist of three terms: a decay term, an input term, and an adaption term. The input term integrates the activity over space and an external input $P(x,t)$. $H(\cdot)$ is the Heaviside function; when the input term is large enough (i.e., when it exceeds k) the term becomes non-zero. The dynamics of $q(x,t)$ depend linearly on both variables. We assume that the adaption occurs more slowly than the activity, and fix $\delta = \alpha/10$. We interpret $u(x,t)$ as representing the activity of a cortical column, and $q(x,t)$ as an adaptation term that acts as a local feedback mechanism to depress the synaptic drive.

At the spatial scale of the LFP, seizure dynamics exhibit complex spatiotemporal patterns (Wagner et al. 2015; Smith et al. 2016). In González-Ramírez et al. (2015), we considered the large amplitude traveling wave dynamics near seizure termination. The main features replicated by the model were the wave speed and width (as obtained through the procedures developed in González-Ramírez et al. 2015). A third additional feature, labeled the "reverberation" in González-Ramírez et al. (2015), consisted of a smaller amplitude fluctuation or

"reverberation" of activity that followed the large amplitude waves. Here, we focus our analysis on the wave features and ranges of parameters obtained from five seizures in two patiens (Patient 1 and Patient 2 in González-Ramírez et al. 2015). For these two patients, the observed speeds vary from approximately 80 μm/ms to 500 μm/ms, the observed widths vary from approximately 2000 μm to 5000 μm, and the reverberation times (i.e., the time between the first large amplitude wave and the smaller amplitude reverberation) vary from approximately 30 ms to 230 ms.

In González-Ramírez et al. (2015), the authors studied the existence and stability of traveling wave solutions of the model (1). Depending on the model parameters, the linearization of the associated system in the moving coordinate frame ($z = x - ct$, for speed $c > 0$) consists of either purely real or complex eigenvalues. In both cases, the solution consists of a pulse followed by a depression of activity due to the linear adaptation term. In the real eigenvalue case, the activity returns monotonically to rest. In the complex eigenvalue case, the activity returns to rest by means of damped oscillations. These damped oscillations produced features consistent with the "reverberation" of activity observed *in vivo* (see González-Ramírez et al. 2015 for details). Thus, to produce features consistent with the *in vivo* data, the model solutions were restricted to the complex eigenvalue case. Using this restriction, the authors obtained ranges of parameters for wave propagation consistent with the clinical data near seizure termination (Table 1). In what follows, we fix the four model parameters in the ranges defined in Table 1, and examine the impact on the model dynamics of including an inhibitory neural population.

2 Activity-based model with excitatory and inhibitory populations and a linear adaptation term

The original model (1) consists of an excitatory neural field with a linear adaptation term directly regulating the excitatory population. Given the choice and position of the adaptation term, this simple model reproduces important features observed in human clinical data recorded near seizure termination (i.e., wave speed, width and

Table 1 Parameter ranges supporting wave propagation consistent with the *in vivo* data, fixing $\delta = \alpha/10$

Patient	α	β_0	σ (μm)	k
1	0.6–2.3	2.025–2.5	40–250	0.15–0.17
2	0.6–3.1	2.025–2.3	20–600	0.16–0.18

For simplicity, the units for α have been rescaled to non-physical units (1 α-unit = 25 Hz). From (González-Ramírez et al. 2015)

"reverberation" of activity) (González-Ramírez et al. 2015). We now propose a modified model that includes an inhibitory population:

$$\begin{aligned}
\frac{du_e}{dt}(x,t) &= -\alpha_e u_e(x,t) + \alpha_e S_e\left(G_{ee}\otimes u_e(x)\right.\\
&\quad \left. -G_{ie}\otimes u_i(x) + P(x,t) - k_e\right) - \alpha_e\beta_0 q(x,t)\\
\frac{dq}{dt}(x,t) &= \delta u_e(x,t) - \delta q(x,t)\\
\frac{du_i}{dt}(x,t) &= -\alpha_i u_i(x,t) + \alpha_i S_i\left(G_{ei}\otimes u_e(x)\right.\\
&\quad \left. -G_{ii}\otimes u_i(x) + Q(x,t) - k_i\right), \qquad (2)
\end{aligned}$$

where $u_e(x,t)$ and $u_i(x,t)$ are the excitatory and inhibitory synaptic drives, respectively, which serve as measures of neural population activity (Pinto et al. 1996; Ermentrout and Terman 2010). Here, we interpret the state $u_e(x,t) = 0$, $u_i(x,t) = 0$ and $q(x,t) = 0$ as a resting state of low-level background activity. Negative values therefore indicate a depression of activity below this baseline (Wilson and Cowan 1973) (See Supplemental Material). As mentioned above and shown in González-Ramírez et al. (2015), the adaptation term $q(x,t)$ supports damped oscillations necessary to reproduce the "reverberation" of activity observed in the clinical data. $P(x,t)$ and $Q(x,t)$ are external inputs to the excitatory and inhibitory populations, respectively, and the convolutions that determine the spatial interactions are defined by,

$$G_{jk}\otimes w(x) = \frac{g_{jk}}{2\sigma_{jk}}\int_{-\infty}^{+\infty} e^{-\frac{|x-y|}{\sigma_{jk}}} w(y,t)\,dy \qquad (3)$$

We focus the mathematical analysis on the case where S_e and S_i are Heaviside functions, which become non-zero when the synaptic input exceeds a given threshold k_j, where $j = \{e,i\}$. In this way we obtain a piecewise-linear system which is analytically tractable and from which we can constrain parameters in terms of the matching conditions (i.e., conditions obtained when the Heaviside function becomes non-zero). Once the parameter ranges are determined for the Heaviside function we extend the analysis of the model and compute numerical simulations replacing S_e and S_i with more general sigmoid functions for which analytic solutions are not available.

The parameters of model (2) are defined as follows: α_e and α_i are the decay parameters for the activity term of the excitatory and inhibitory populations, respectively, and δ is the decay parameter for the adaptation term. The parameters σ_{jl}, for $\{j,l\} = \{e,i\}$, account for the spatial decay of the synaptic connectivity within and between excitatory and inhibitory populations. The parameters k_j, for $j = \{e,i\}$, account for the synaptic threshold of each population, and β_0 represents the strength of the adaptation term on the excitatory population.

In analyzing the model (2) we make the following assumptions: **i)** The medium is homogeneous and the parameters remain constant in space and time. **ii)** The effect of the inhibitory population remains spatially localized, i.e., in the model the spatial connectivity between the inhibitory population and the excitatory and inhibitory populations has an extent of $\sigma_{il} = 100\ \mu$m, for $l = \{e, i\}$. This assumption of spatially local inhibition is motived by experimental observations (e.g., Markram et al. 2004). For simplicity we assume $g_{ie} = g_{ii}$ so that changes in a single parameter can be used to analyze the effect of inhibition on the wave properties. We note that this change is qualitatively consistent with more detailed models of a cortical column, in which superficial layer excitatory and inhibitory cells - regular spiking pyramidal cells and basket cells, respectively - receive the same number of inputs from superficial basket cells (Traub et al. 2005). **iii)** The extent of the excitatory connectivies (σ_{ee} and σ_{ei}) varies between 100 μm to 1 mm. This is in agreement with the parameter ranges obtained in González-Ramírez et al. (2015) as well as with experimental observations (Wilson and Cowan 1973; Braitenberg and Schuz 1998). We also assume that the strength of the excitatory interactions are fixed $g_{ee} = g_{ei} = 1$. **iv)** Given the presence of a reverberation of activity in the clinical data, we focus our analysis on the traveling wave solutions of the excitatory population determined by the complex eigenvalue case; we note this case requires $\beta > \frac{(\delta-\alpha)^2}{4\delta}$ where $\beta = \alpha\beta_0$ and α and β_0 are as in Table 1 and $\delta = \alpha/10$ (see González-Ramírez et al. 2015). Thus, we restrict our analysis to the parameter ranges previously determined from the clinical data for model (1). In this way the reverberation of activity is approximated by the damped oscillations present in the traveling wave solution of the excitatory population. Our goal here is to study the impact of inhibition on these traveling wave solutions. Also, to simplify our notation, we use nondimensional units for the decay rates of the excitatory and inhibitory populations (α_e and α_i), where 1-α unit = 25 Hz. **v)** We assume that there is no external or long-range input to the inhibitory population, i.e., $Q(x, t) = 0$. Under this assumption, the inhibitory population only activates in response to nearby excitatory activity. **vi)** We are interested in wave propagation with speeds varying from 80 μm/ms to 500 μm/ms, and widths varying from 1000 μm to 5000 μm, as deduced from the human clinical recordings in González-Ramírez et al. (2015), and in agreement with other observations (Golomb and Amitai 1997; Chervin et al. 1988; Wadman and Gutnick 1993; Wu et al. 2001).

2.1 Traveling wave solutions

Our goal is to study the existence of traveling waves of high amplitude in model (2). To do so, we rewrite the equations in a moving coordinate frame $z = x - ct$, with $c > 0$, and find stationary solutions of this system; these solutions move with a constant speed c, a constant width w, and fixed shape. Since (2) is a piecewise linear differential system, we can obtain explicit solutions for the traveling waves. To do so, we assume the existence of pulses of activity for both populations. For these pulse solutions, the threshold of the excitatory and inhibitory population (k_e and k_i) is crossed exactly twice. We assume that the points at which the threshold is crossed, i.e., where the Heaviside function is activated/deactivated, are determined by $x = \{w_{e0}, w_{ef}\}$, and $x = \{w_{i0}, w_{if}\}$, for the excitatory and inhibitory population, respectively. We also assume that an initial wave of excitation is followed by a wave of inhibition i.e., $w_{if} \leq w_{ef}$, and once the excitatory wave ends and the activity returns to the rest state, so will the activity of the inhibitory population, thus $w_{i0} \leq w_{e0}$. In Fig. 3 we explore the last assumption and motivate the simplifying assumption $w_{i0} = w_{e0}$. We note, however, the possibility of wave solutions for $w_{i0} > w_{e0}$. In order to focus on the qualitative properties of wave propagation we concentrate on the case $w_{i0} = w_{e0}$. This assumption is motivated by the physical intuition that when excitatory activity ceases, so does the inhibitory activity. These assumptions establish the "matching conditions" and hence the relationship between parameters to determine the existence of wave solutions with a given speed and width. The width of the excitatory wave is therefore determined by $w_{ef} - w_{e0}$, and the width of the inhibitory wave is determined by $w_{if} - w_{i0}$. To simplify notation, and given that the wave solution is translationally invariant we set $w_{e0} = 0$, and $w_{ef} = w$. At w and w_{if} the argument to the Heaviside function is zero, that is, the synaptic threshold is achieved. At this point the activity of both populations is zero. At smaller z values the synaptic term in the model becomes non-zero, and the activity of both populations starts to exponentially increase as the wave begins to propagate. At w_{e0} and w_{i0} the synaptic threshold is again reached and the Heaviside functions in both populations become zero, so that synaptic input is deactivated. The activity then returns to baseline after the wave has passed. The activity returns to rest monotonically for the inhibitory population and as a damped oscillation for the excitatory population.

By solving the corresponding traveling wave system we find that the wave profile (i.e., the wave shape) is not affected by the inhibitory interaction. This is because the effect of inhibition is inside the Heaviside term and therefore only acts to determine whether the total synaptic input is above or below the threshold. The inhibition, however, does impact other wave properties, such as the speed and width, by affecting the matching conditions (for details see the Supplemental Material). We therefore obtain the same wave profile for the excitatory

population as derived in González-Ramírez et al. (2015). For completeness, we repeat the solution here:

$$u_e(z) = \begin{cases} 0 & \text{if } z \geq w \\ v_e(z-w)\,(c_3\cos(z\phi) + c_4\sin(z\phi)) + \frac{\alpha_e}{\alpha_e+\beta} & \text{if } 0 < z < w \\ v_e(z)\,(c_1\cos(z\phi) + c_2\sin(z\phi)) & \text{if } z \leq 0 \end{cases} \quad (4)$$

where

$$v_e(z) = \frac{\alpha_e e^{(\frac{\alpha_e+\delta}{2c})z}}{(\alpha_e+\beta)\sqrt{4\delta\beta-(\delta-\alpha_e)^2}}, \qquad \phi = \frac{\sqrt{4\delta\beta-(\delta-\alpha_e)^2}}{2c}$$

$$c_1 = \sqrt{4\delta\beta-(\delta-\alpha_e)^2} + \exp\left(-w\frac{\alpha_e+\delta}{2c}\right) \times \left[(2\beta+\alpha_e-\delta)\sin(w\phi) - \sqrt{4\delta\beta-(\delta-\alpha_e)^2}\cos(w\phi)\right]$$

$$c_2 = (2\beta+\alpha_e-\delta) + \exp(-w\frac{\alpha_e+\delta}{2c}) \times \left[-(2\beta+\alpha_e-\delta)\cos(w\phi) - \sqrt{4\delta\beta-(\delta-\alpha_e)^2}\sin(w\phi)\right]$$

$$c_3 = (2\beta+\alpha_e-\delta)\sin(w\phi) - \sqrt{4\delta\beta-(\delta-\alpha_e)^2}\cos(w\phi)$$

$$c_4 = -(2\beta+\alpha_e-\delta)\cos(w\phi) - \sqrt{4\delta\beta-(\delta-\alpha_e)^2}\sin(w\phi).$$

For the inhibitory population we obtain:

$$u_i(z) = \begin{cases} 0 & \text{if } z \geq w_{if} \\ 1 - e^{\frac{\alpha_i}{c}(z-w_{if})} & \text{if } w_{i0} < z < w_{if} \\ e^{\frac{\alpha_i}{c}z}\left(e^{-\frac{\alpha_i}{c}w_{i0}} - e^{-\frac{\alpha_i}{c}w_{if}}\right) & \text{if } z \leq w_{i0}. \end{cases} \quad (5)$$

The existence of waves for the excitatory and inhibitory populations is determined by the matching conditions, i.e., the points at which the interactions of the excitatory and inhibitory population equal the threshold of the Heaviside function. Considering no external inputs (i.e., $P(x,t) = 0$ and $Q(x,t) = 0$), the matching conditions for the excitatory and inhibitory population are:

$$G_{ee} \otimes u_e(x) - G_{ie} \otimes u_i(x) = k_e, \text{ where } x = 0 \text{ and } x = w, \quad (6)$$

$$G_{ei} \otimes u_i(y) - G_{ii} \otimes u_i(y) = k_i, \text{ where } y = w_{i0} \text{ and } y = w_{if}. \quad (7)$$

In what follows, we use these matching conditions to explore the influence of inhibition on the existence of excitatory wave solutions with the desired properties of width, speed and reverberation consistent with the clinical data.

To illustrate a traveling wave solution of the model (2), we fix all of the parameters and solve the matching conditions in Eqs. (6) and (7). Examples of the resulting traveling waves for the excitatory and inhibitory populations are plotted in Fig. 1. We note that the profile of the excitatory wave consists of a sudden increase in activity (near $w = 2000$ μm) followed by a depression of activity due to the adaptation term; in this example, we observe damped oscillations in the excitatory activity due to the complex eigenvalues of the solution. We also note that the peak of the inhibitory wave exceeds the peak of the excitatory wave; for the choice of $g_{ii} = g_{ie} = 1$, the inhibitory activity reaches a peak of 1, while the excitatory activity reaches a maximum of 0.8. The reason for this difference is that the inhibitory population lacks an adaptation term. At $x = 0$ μm in Fig. 1, the matching conditions of the excitatory population (6) fall bellow the threshold of the Heaviside function (at w_{e0}). The excitatory wave profile is followed by a depression of activity due to the adaptation term, and the effect of the excitatory-to-inhibitory interaction is reduced (after w_{e0}), which causes the inhibitory population to fall below the threshold of the Heaviside function (7).

2.2 On the existence of excitatory and inhibitory waves

We recall that traveling wave solutions are determined by the properties of the excitatory population, adaptation term and inhibitory population. For the excitatory population there are eight free parameters: activity decay rate (α_e), excitatory connectivity extent (σ_{ee} and σ_{ei}), excitatory connectivity strength (g_{ee} and g_{ei}), excitatory synaptic threshold (k_e), and excitatory activation/deactivation points of the Heaviside function (w_{e0} and w_{ef}). For the adaptation term we have two free parameters: adaptation decay rate (δ) and adaptation strength (β). For the inhibitory population we have eight free parameters: activity decay rate (α_i), inhibitory connectivity extent (σ_{ie} and σ_{ii}), inhibitory connectivity strength (g_{ie} and g_{ii}), inhibitory synaptic threshold (k_i), and inhibitory activation/deactivation points of the Heaviside function (w_{i0} and w_{if}). Due to the inclusion of the inhibitory population we have the addition of ten new parameters in comparison to González-Ramírez et al. (2015) in which fewer parameters were present. Given the presence of these new parameters the difficulty for determining ranges of parameters that support wave propagation is increased. To explore the range of parameters that support traveling waves, we proceed as follows:

– First, we consider a simpler scenario in which the excitatory and inhibitory populations possess the same characteristics, i.e., $\sigma_{ee} = \sigma_{ei}$, $\sigma_{ie} = \sigma_{ii}$, $k_e = k_i$, $\alpha_e = \alpha_i$, $w_{i0} = w_{e0}$ and $w_{if} = w_{ef}$. We then explore

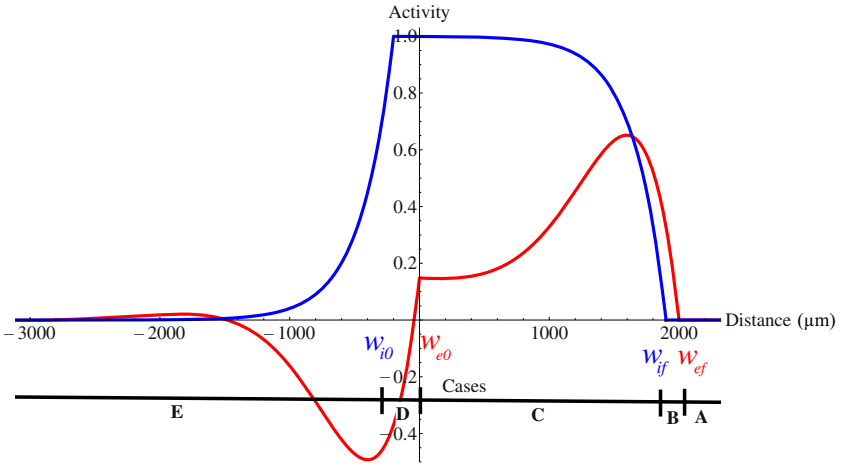

Fig. 1 An example of a traveling wave solution of the excitatory (red) and inhibitory (blue) population. In this figure $\alpha_e = \alpha_i = 1$, $\delta = 0.1$, $\beta = 5.0$, $\sigma_{ee} = \sigma_{ei} = 300\ \mu$m, $\sigma_{ie} = \sigma_{ii} = 100\ \mu$m, $g_{ie} = g_{ii} = 1$, $c = 250\ \mu$m/ms, $w_{e0} = 0\ \mu$m, $w_{ef} = w = 2000\ \mu$m, $w_{i0} = -200\ \mu$m and $w_{if} = 1900\ \mu$m. We show a snapshot of the traveling wave in the moving coordinate frame (u_e vs z, and u_i vs z, where $z = x - ct$). As time evolves wave moves to the right. We observe damped oscillations toward the rest state. These damped oscillations are due to the complex eigenvalues obtained in the traveling wave system and were used to restrict parameters for wave propagation in González-Ramírez et al. (2015) (see Supplemental Material for details)

the relationships between wave width and speed that support wave propagation (see Fig. 2). In addition, we formally study the linear stability of these traveling wave solutions through the construction of an Evans Function (see Supplemental Material).

– Second, we assume that excitatory wave propagation induces inhibitory wave propagation (i.e., $w_{if} < w_{ef}$). We explore the effect of changing the deactivation point of the Heaviside function for the inhibitory population (i.e., changing w_{i0} relative to a fixed w_{e0}) while we increase the inhibitory strength. We also explore the effect of different inhibitory population timescales relative to the excitatory population timescale (i.e., $\alpha_i = \frac{\alpha_e}{10}$, $\alpha_i = \alpha_e$ and $\alpha_i = 10\alpha_e$) while the remaining parameters are fixed (see Fig. 3).

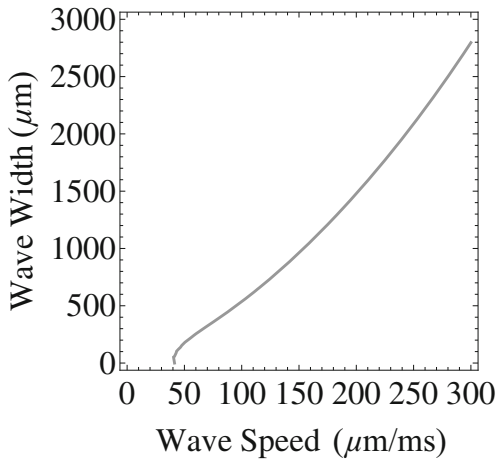

Fig. 2 Relationship between wave speed and wave width of the excitatory and inhibitory population assuming that both populations have the same properties. In this figure we fix $\alpha_e = \alpha_i = 1$, $\delta = 0.1$, $\sigma = 100\ \mu$m, $\beta = 2.1$, $g_i = 0.25$, $w_{i0} = w_{e0} = 0\ \mu$m, $w_{if} = w_{ef} = w$ and vary $k_e = k_i$

– Third, motivated by the previous analysis, we make additional assumptions that further simplify the model (i.e., $w_{e0} = w_{i0}$). We then explore the effect of increasing the inhibitory strength on the existence of wave solutions with the desired conditions on wave speed. At the same time, we analyze the effect of different inhibitory decay rates (α_i) relative to excitatory decay rates (α_e). We assume three possible scenarios: the inhibition acts faster than the excitation, the inhibition acts at the same timescale as the excitation, or the inhibition is slower than the excitation ($\alpha_i = 10\alpha_e$, $\alpha_e = \alpha_i$ and $\alpha_i = \alpha_e/10$, respectively). In this way, we analyze the existence of waves of a given speed by considering distinct inhibitory strength and inhibitory decay rates while the remaining parameters are fixed. To study the existence of wave solutions we look at the curves determined by the matching conditions (6 and 7). In order to establish the existence of waves both matching conditions must be satisfied, i.e., we are interested in the intersection of the curves determined by the matching conditions. Thus, we examine how the matching conditions are affected by changes in the inhibitory strength and inhibitory decaying rate (see Fig. 4).

– Fourth, we perform a similar study as described in the previous point but we now fix the wave width. Thus, we study the existence of waves of a given width by considering distinct inhibitory strength and inhibitoy decay rates while the remaining parameters are fixed. We do this by analyzing the intersections of

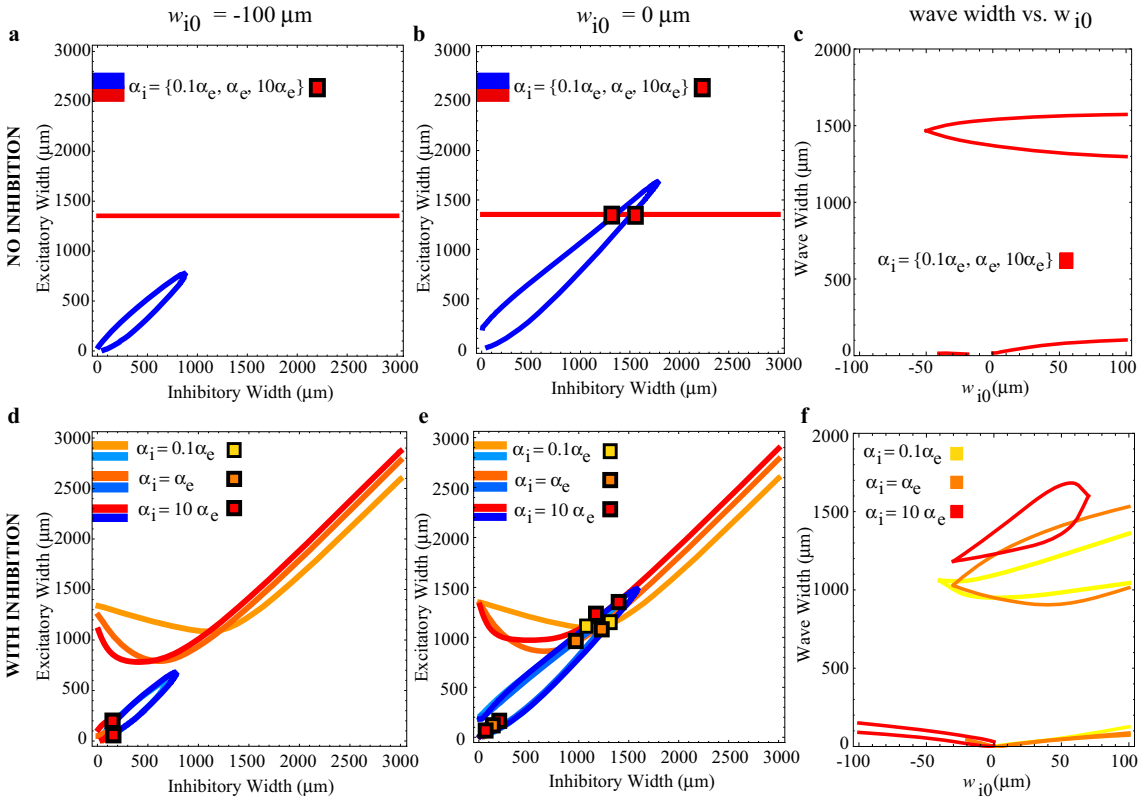

Fig. 3 Traveling wave solutions tend to exist when the excitatory and inhibitory interactions become inactive at the same point in space. Relationship between the width of the excitatory wave (w) and the inhibitory wave (w_{if}) determined by the matching conditions for different choices of the deactivation point of inhibition w_{i0}, strength of inhibition g_{ie}, and decay rate of the inhibitory population α_i. In subfigures (**a**), (**b**), (**d**) and (**e**), the red and blue curves represent solutions satisfying the excitatory and inhibitory matching conditions, respectively. Squares indicate intersections of the matching conditions for a given choice of α_i. At these intersections waves exist with the given excitatory and inhibitory width. In subfigure (**a**, **b**) inhibition is off (i.e., $g_{ie} = 0$). In subfigure (**d**, **e**) inhibition is active ($g_{ie} = g_{ii} = 0.2$) and we explore three possibilities: the inhibition is slower than the excitation ($\alpha_i = 0.1\alpha_e$), the inhibition has the same timescale as the excitation ($\alpha_i = \alpha_e$), or the inhibition is faster than the excitation ($\alpha_i = 10\alpha_e$); see legends in each subfigure. In (**a**, **d**), $w_{i0} = -100\ \mu$m. In (**b**, **e**), $w_{i0} = 0\ \mu$m. The different colors represent different decay rates for the inhibitory population. We fix the parameters: $\delta = \frac{\alpha_e}{10}$, $\beta = 2.1$, $g_{ee} = g_{ei} = 1$, $\sigma_{ee} = 200\ \mu$m, $\sigma_{ie} = \sigma_{ii} = 100\ \mu$m and $c = 200\ \mu$m/ms. **c**, **f** We follow the intersections found in (**a**, **b**) and (**d**, **e**), respectively, as we modify the parameter w_{i0}. In (**a**) there are no intersections of the excitatory and inhibitory matching condition curves. In (**b**) and (**d**) there are two intersections of the excitatory and inhibitory solution curve. In (**e**) there are six intersections for wide waves and three for narrow waves. We note that with inhibitory synapses active (**f**), the width of the waves are determined by both w_{i0} and the timescale of inhibition. In particular, for values of w_{i0} closer to 0, wide waves exist in our range of interest

the matching conditions, which specify the existence of waves with given conditions (see Fig. 5). At intersections of the matching conditions waves exist with the given excitatory and inhibitory width. We explore three possibilities: the inhibition is one order of magnitude slower than the excitation ($\alpha_i = 0.1\alpha_e$), the inhibition acts at the same timescale as excitation ($\alpha_i = \alpha_e$) or the inhibition acts an order of magnitude faster than the excitation ($\alpha_i = 10\alpha_e$).

– Fifth, we summarize the effect of increasing the inhibitory strength and inhibitory decay rate on the existence of waves by analyzing the changes in the wave speed and width determined by the matching conditions. Here, instead of analyzing the matching conditions we focus on their intersections. In this way, we explore the relationship between wave speed and wave width determined by the conditions set by the rest of the parameters (see Figs. 4c, f, i, 5c, f, i and 6).
– Sixth, we perform numerical simulations of the model to corroborate the results found in the previous analysis (see Fig. 7).

To begin our analysis, we focus on a simple scenario in which the excitatory and inhibitory populations have the same synaptic characteristics, connectivity, and activation/deactivation points for the Heaviside function (i.e., $\sigma_{ee} = \sigma_{ei}$, $\sigma_{ie} = \sigma_{ii}$, $w_{i0} = w_{e0}$ and $w_{e0} = w_{ef}$). In this scenario, the excitatory and inhibitory wave solutions have the same speed and width. Moreover the matching conditions (6 and 7) reduce to one equation. In Fig. 2 we explore the relationship between speed and width of

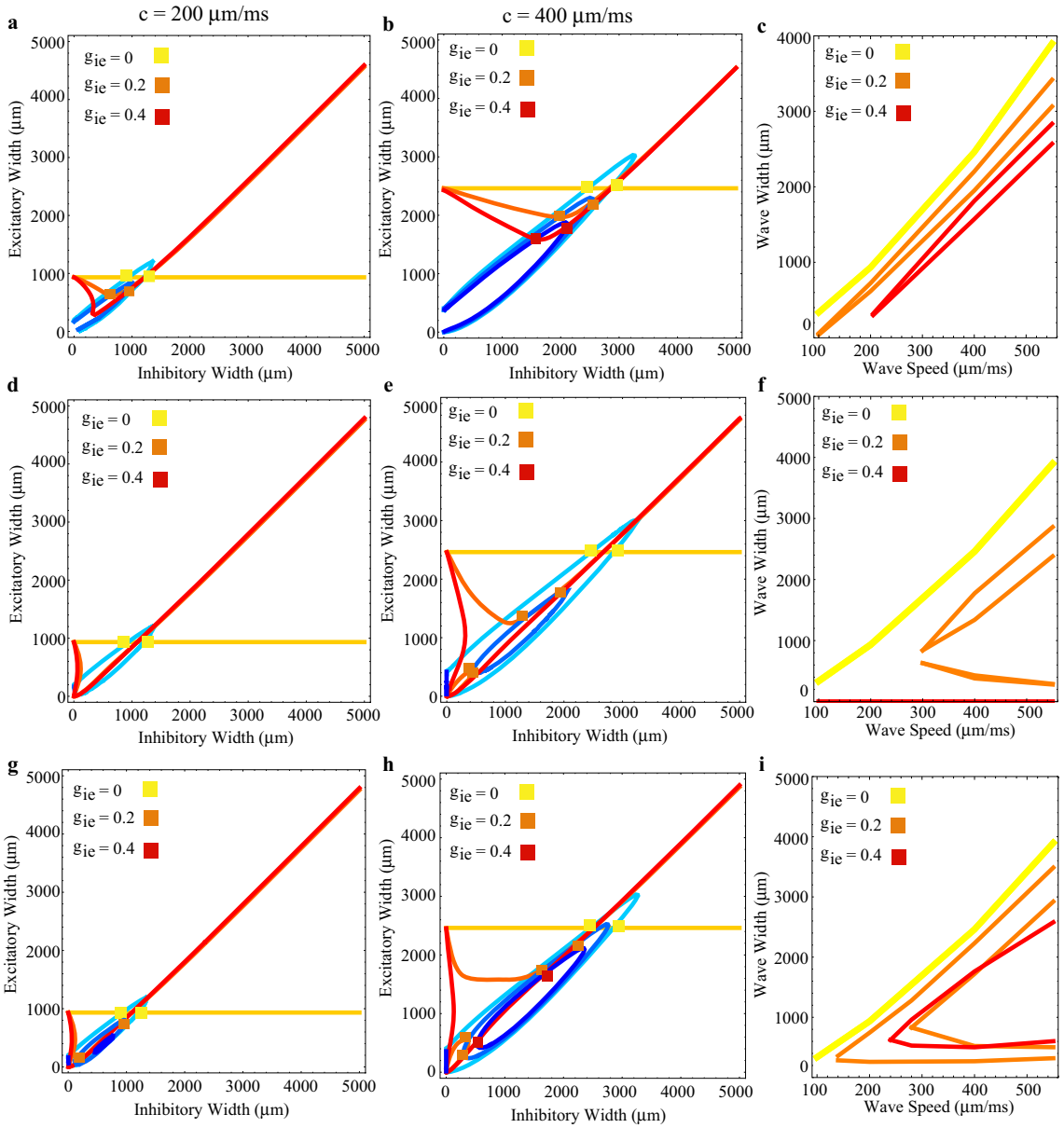

Fig. 4 Traveling waves consistent with the *in vivo* data tend to exist when inhibition is weak. Relationship between the width of the excitatory wave (w) and the width of the inhibitory wave (w_{if}) determined by the matching conditions (6) and (7) for different values of c, g_{ie} and α_i. The red and blue curves in the first and second column represent the matching conditions for the excitatory and inhibitory population, respectively. Each different color represents a different strength of inhibition (see legend). The boxes represent the intersections of the matching conditions. Each row represents a different timescale for the inhibitory population. First row, $\alpha_i = \alpha_e/10$; second row, $\alpha_i = \alpha_e$; third row, $\alpha_i = 10\alpha_e$. The first and second columns represent different speeds for the excitatory population: first column, $c = 200$ μm/ms; second column, $c = 400$ μm/ms. The third column shows the existence of waves (i.e., the colored boxes) for a fixed inhibitory strength as the speed c is increased. Other model parameters were fixed at: $\sigma_{ee} = 500$ μm, $\sigma_{ie} = 100$ μm, β =2.1, $\alpha_e = 1$ and $\delta = \alpha_e/10$. We note the qualitatively similar behavior for the three timescales. In general, for fixed wave speed the waves tend to be narrower as the inhibitory effect is increased. At a slow inhibitory timescale, there exists broader range of waves in the interval of interest over stronger inhibitory strengths (**c**) compared to faster inhibitory timescales (**f**, **i**)

the excitatory/inhibitory waves in this simplified case. We note that there are two branches of waves, one of which specifies fast and wide waves whereas the other specifies slow and thin waves. We explore the existence of these wave solutions in the Supplementary Material, and formally establish the linear stability of the fast and wide waves and the linear instability of the narrow and slow waves (see Supplemental Material for details).

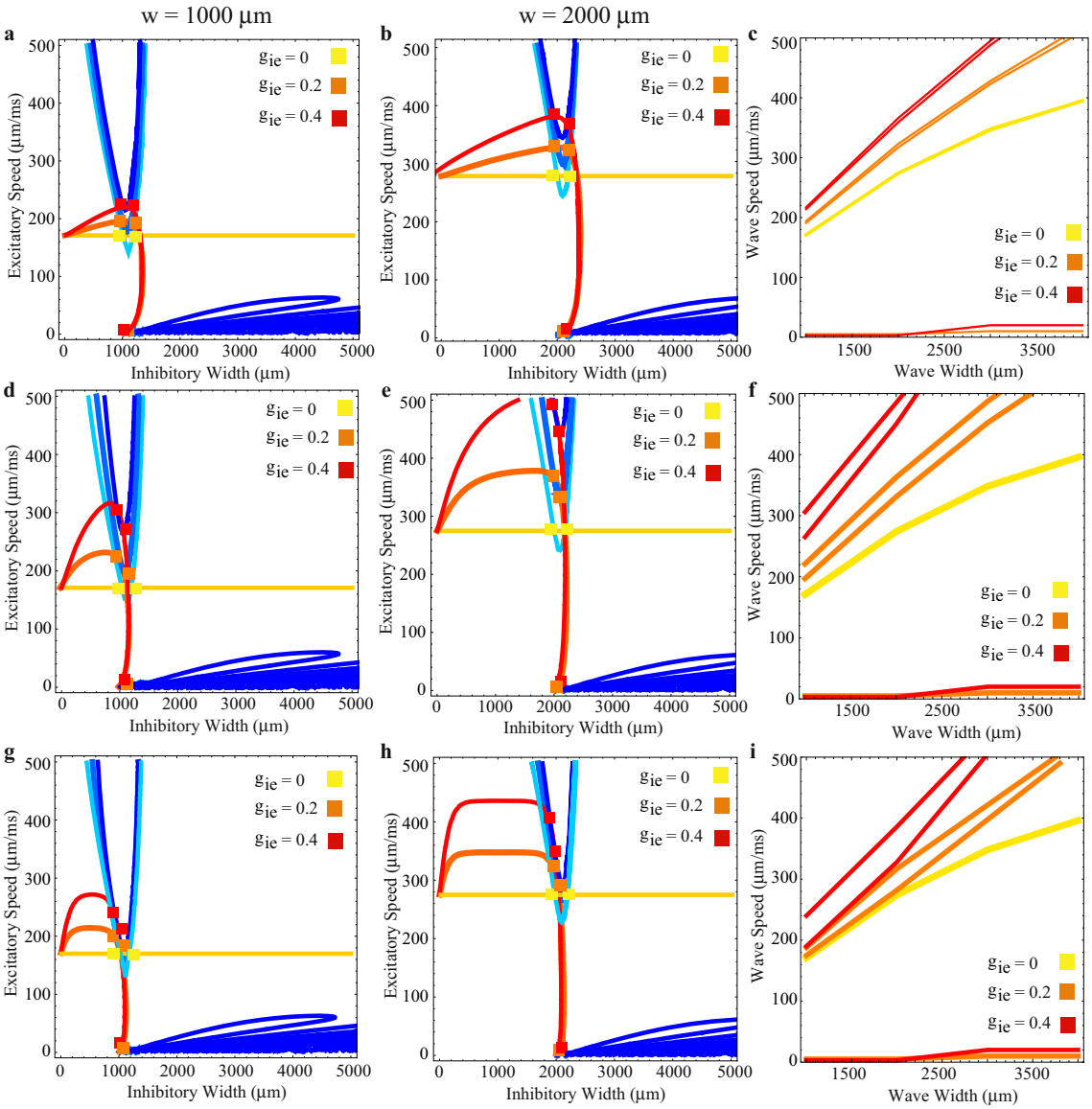

Fig. 5 Traveling wave solutions exist in the physical range of interest for relatively weak inhibitory strengths. Relationship between the speed of the excitatory wave and the width of the inhibitory wave determined by the matching conditions (6) and (7) for different values of the excitatory wave width w and the strength of inhibition g_{ie}. In the first and second column the red and blue curves represent the matching conditions for the excitatory and inhibitory population, respectively. Each color indicates a different strength of inhibition (see legend). Each row represents a different timescale for the inhibitory population. First row, $\alpha_i = \alpha_e/10$; second row, $\alpha_i = \alpha_e$ and third row, $\alpha_i = 10\alpha_e$. Traveling wave solutions are indicated by colored boxes. The first and second column represent different widths for the excitatory population: first column, $w = 1000\ \mu$m and second column, $w = 2000\ \mu$m. The third column shows the existence of waves (i.e., the colored boxes) for a fixed inhibitory strength as the width w is increased. Parameters were fixed at $\sigma_{ee} = 200\ \mu$m, $\sigma_{ie} = 100\ \mu$m, β =2.3, $\alpha_e = 1$ and $\delta = \alpha_e/10$. We note that there is a qualitatively similar behavior for the three timescales. In general, as the wave width is increased and the inhibitory strength is increased the waves tend to be faster. However, a slower inhibitory timescale effect (**c**) shows a slightly broader existence of waves in the range of interest for stronger inhibitory effects compared to faster inhibitory timescales (**f**) and (**i**)

2.3 Effect of the choice of deactivation of inhibition (w_{i0})

The example in Fig. 1 illustrates the wave profile of the excitatory and inhibitory populations. To further explore the impact of inhibition, we examine how variations in the parameters of inhibition impact the solutions to the matching conditions (6) and (7). We focus our analysis on three inhibitory parameters: w_{i0}, the deactivation point of inhibition (i.e., the point at which the Heaviside function becomes zero); $g_{ie} = g_{ii}$, the strength of inhibitory activity on the neural populations; and α_i, the decay rate

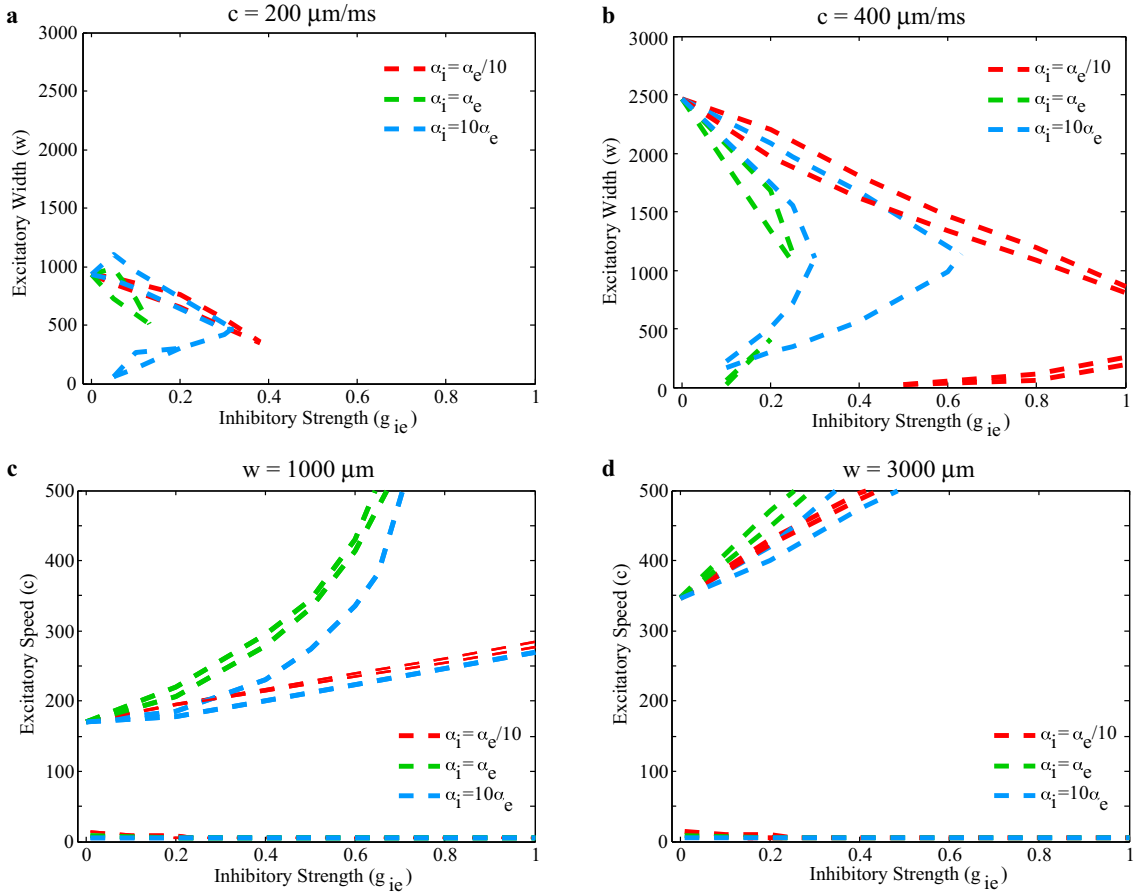

Fig. 6 Traveling wave solutions exist when inhibition is weak and slow. **a–b** Wave solutions as a function of excitatory width (w), strength of inhibition ($g_{ie} = g_{ii}$), and inhibitory decay rate (α_i) with wave speeds: **a** $c = 200$ μm/ms, and **b** $c = 400$ μm/ms. **c–d** Wave solutions as a function of excitatory speed (c), strength of inhibition ($g_{ie} = g_{ii}$), and inhibitory decay rate (α_i) with wave widths: **d** $w = 1000$ μm, and **e** $w = 3000$ μm. The line colors indicate different values of inhibitory decay rate (see legends). Fixed parameters in first row: $\sigma_{ee} = \sigma_{ei} = 500$ μm, $\sigma_{ie} = \sigma_{ii} = 100$ μm, $\alpha_e = 1$, and $\beta = 2.1$. Fixed parameters in second row: $\sigma_{ee} = \sigma_{ei} = 200$ μm, $\sigma_{ie} = \sigma_{ii} = 100$ μm, $\alpha_e = 1$, and $\beta = 2.3$

of inhibition. We fix the other model parameters at values consistent with the *in vivo* traveling waves (as in González-Ramírez et al. 2015). In Fig. 3 we show solutions of the matching conditions (6) and (7) for different choices of w_{i0}, g_{ie}, and α_i. The red and blue curves indicate the solutions to the excitatory and inhibitory matching conditions, respectively. That is, the red (blue) curves indicate pairs of widths (w, w_{if}) for which a solution to the excitatory (inhibitory) matching conditions exists. We are interested in the intersection of these two curves, as these intersections indicate parameter values for which both excitatory and inhibitory matching conditions are satisfied. In what follows, we explore the change in the widths of the excitatory and inhibitory waves of the model solutions due to changes in the inhibitory properties (w_{i0}, g_{ie}, and α_i). In the first row (Fig. 3a–b) we consider the case $g_{ie} = g_{ii} = 0$, i.e., there is no influence of the inhibitory population on either neural population. Therefore, solving the matching conditions for the excitatory population produces the horizontal red lines in Fig. 3a–b; regardless of the width of the inhibitory wave, the value of w_{i0}, or the inhibitory rate α_i, the width of the excitatory wave is not affected. However, the excitatory population does influence the inhibitory population (i.e., $g_{ei} \neq 0$). Solving the matching conditions for the inhibitory population (7) produces the blue curves in Fig. 3a–b. Inspection of Fig. 3a–b shows that the width of the excitatory wave affects the choice of the inhibitory width that satisfies Eq. (7). As the value of w_{i0} decreases (i.e., as the choice of the deactivation point of inhibition gets farther away from $w_{e0} = 0$, the deactivation point of excitation) we find that the solution curve that satisfies Eq. (7) (i.e., the blue curve in Fig. 3a–b) gets smaller. Therefore, the relationship between inhibitory and excitatory wave width that satisfies Eq. (7) becomes more restricted. That is, as the value of w_{i0} decreases from $w_{e0} = 0$ (see Fig. 1) so does the inhibitory width, and the initial activation point of the inhibitory activity (w_{if}). We summarize the effect of different choices of w_{i0} in Fig. 3c.

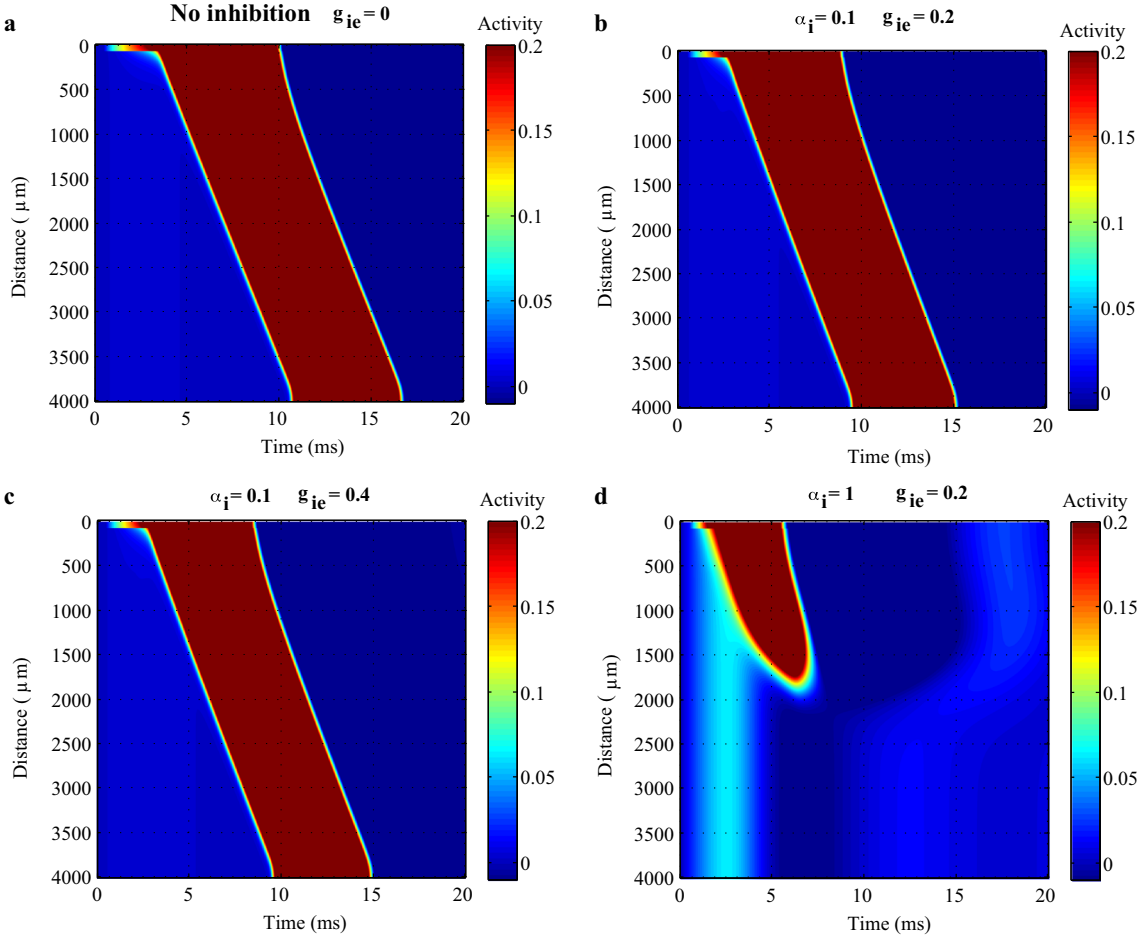

Fig. 7 Numerical simulations support the conclusion that strong inhibition disrupts wave propagation in the model. In each figure, we plot the activity (color) versus distance and time. An initial perturbation near $t = 0$ s, distance $= 0$ μm starts the traveling waves. The simulations in all figures have the fixed parameters: $\beta = 2.5$, $\alpha_e = 1$, $\delta = 0.1$, $\sigma_{ee} = \sigma_{ei} = 600$ μm and $\sigma_{ie} = \sigma_{ii} = 100$ μm and we vary the parameters k_e, $g_{ie} = g_{ii}$ and α_i. **a** We fix $g_{ie} = g_{ii} = 0$ and $k_e = 0.105$. **b** In the case of slow-acting, weak inhibition, we fix $\alpha_i = 0.1$, $g_{ie} = 0.2$ and $k_e = 0.1$. **c** In the case of slow-acting, strong inhibition, we fix $\alpha_i = 0.1$, $g_{ie} = 0.4$ and $k_e = 0.1$. **d** In the case of fast-acting, weak inhibition we fix $\alpha_i = 1$, $g_{ie} = 0.2$ and $k_e = 0.064$ to obtain a wave that fails to propagate after 5 ms

In this plot we vary values of w_{i0} between -100 to 100 and plot the intersection points i.e., the existence of waves as previously described. We observe that the solutions of Eqs. (6) and (7) intersect when w_{i0} is closer to $w_{e0} = 0$. We also show in this figure how the solution curves change due to different choices of α_i. In this case, the solution curves do not depend on α_i because the inhibitory interactions are disconnected (i.e., $g_{ie} = g_{ii} = 0$). We find for values of w_{i0} close to 0 the same number of intersection points. Therefore, to simplify our assumptions we choose a value of w_{i0} close to 0.

In Fig. 3d–e we consider the case of synaptically connected inhibition and include a relatively weak value for the strength of inhibition on neural populations (i.e., $g_{ie} = g_{ii} = 0.2$). Compared to the case of no inhibition (horizontal red lines in Fig. 3a–b), we find that the solutions to the excitatory matching condition (red curves) now consist of two types of relationships. First, we find a nearly linear relationship between the excitatory and inhibitory widths of the solutions for inhibitory widths greater than 1000 μm. That is, for sufficiently wide inhibitory waves the excitatory matching conditions consist of states in which there is a nearly equivalence of excitatory and inhibitory wave widths that is preserved as time evolves. This relationship is not affected by the timescale of inhibition (α_i) or w_{i0}. We conclude that wider excitatory waves (width greater than 1000 μm) are more robust, and not affected by the timescale of inhibitory input.

On the other hand, for values of inhibitory wave widths less than 1000 μm the solution to the excitatory wave matching condition becomes nonlinear (concave upwards), and the excitatory wave width increases as the inhibitory wave width decreases. In particular, as the inhibitory wave width tends to zero the excitatory wave width tends to a

limiting value determined by the no inhibition case (the red flat line in Fig. 3a–b). Thus, as the width of the inhibitory wave becomes thinner, it has less impact on the excitatory wave and this wave approaches the properties of waves without inhibition. We note that the timescale of inhibition impacts the concavity of the curved portion of the excitatory matching condition; faster inhibition acts to more rapidly decrease the excitatory width. Physically, the slow-acting inhibition is more delayed so that the excitatory width remains greater compared to fast-acting inhibition. This same qualitative effect appears in the excitatory solutions for different choices of the deactivation point of inhibition (Fig. 3d–e).

We summarize the effect of w_{i0} in the case of synaptically connected inhibition in Fig. 3f. In this plot we vary continuously w_{i0} between -100 to 100. We find that as w_{i0} becomes more negative, i.e., as the choice of the deactivation point of inhibition gets farther away from the deactivation point of excitation ($w_{e0} = 0$), the solutions that satisfy Eq. (7) become even more restricted and lie outside of the range of interest (wave width smaller than 500 μm). Graphically, as w_{i0} gets smaller, the blue solution curves also become smaller (Fig. 3d–e), so it is less likely for an intersection of the inhibitory and excitatory matching conditions to occur. We also note a shrinking of the solution curves of the inhibitory matching conditions as the decay rate increases. Analyzing Fig. 3f we observe for values of w_{i0} greater than 0 similar qualitative features in the intersection of the matching conditions for different inhibitory decay rates. We observe that for fast-acting inhibition (red curve in Fig. 3f) two waves exist in the range of w_{i0} between -30 to 50. For values of w_{i0} greater than 50 we have no intersection points and therefore no waves exist. On the other hand, for slower-acting inhibition (yellow and orange curves in Fig. 3f) two waves exist in the range of interest for negative values of w_{i0} reletivaly closer to 0 and up to 100. This analysis provides an intuition for the inhibitory timescales that support the existence of waves with the desired features. These results motivate a choice of w_{i0} close to 0 as the existence of waves is established for the different timescales of inhibition whether or not we are in the case of synaptically connected inhibition (Fig. 3c and f). We investigate in more detail the effect of the inhibitory timescale on the existence of waves in the next sections. We conclude that in the case of synaptically connected inhibition, similar to Fig. 3a–b, it is more likely for the two solution curves to intersect when w_{i0} is closer to $w_{e0} = 0$.

This analysis of the impact of inhibition on the wave solutions (Fig. 3) reveals the following result: wave solutions tend to exist when w_{i0} is near $w_{e0} = 0$. We also note that two sets of solutions exist for the case of non-zero inhibition: waves of width near 1000 μm, and of width near 200 μm; the latter is well below the range of physical interest. We find that this result holds for different choices of inhibitory timescale (α_i). We therefore restrict our continuing analysis to the condition in which intersections are more likely (i.e., $w_{i0} = w_{e0} = 0$). Physically, this assumption is reasonable; the excitation acts locally in space to drive the inhibitory population. When this drive is lost, the inhibitory population activity decreases.

2.4 Effect of inhibition on waves of fixed speed

To further explore the impact of inhibition on the wave solutions of the model, we consider the effect of inhibitory parameters on excitatory waves of different speed. We again consider solutions to the excitatory and inhibitory matching conditions, here for different choices of wave speed (columns of Fig. 4), inhibitory timescale (rows of Fig. 4), and strength of inhibition (line color). We choose the speeds to explore a range of values observed in the *in vivo* data. In the first and second columns of Fig. 4, the red and blue curves represent the solutions of the matching conditions for the excitatory and inhibitory populations, respectively. The intersections of these two curves (boxes) represent values for which traveling waves exist for the given parameters. That is, since both matching conditions are satisfied, the existence of excitatory and inhibitory waves is established at these intersections. These intersection points are summarized in third column of Fig. 4 for each timescale of inhibitory activity (each row).

In Fig. 4a we consider the existence of waves with slow-acting inhibition (i.e., $\alpha_i = \alpha_e/10$), a fixed speed of $c = 200$ μm/ms, and varying strengths of inhibition (g_{ie} and g_{ii}, where $g_{ie} = g_{ii}$). When there is no inhibition (i.e., $g_{ie} = g_{ii} = 0$) we find that the excitatory matching condition is a horizontal line (yellow line) as expected when inhibition does not impact the excitatory population. We find in this case that the excitatory and inhibitory (light blue curve) solution curves intersect, which indicates the existence of waves for this choice of parameters. Upon increasing the inhibitory strength (orange and darker blue curves, denoting $g_{ie} = g_{ii} = 0.2$) we find that the excitatory matching (6) condition varies with the wave widths in a similar manner as observed in Fig. 3; after an initial decrease, the excitatory width increases approximately linearly with the inhibitory width for this matching condition. We note that as the inhibitory wave width approaches zero the excitatory width tends to the no inhibition case (as described in Fig. 3). For the inhibitory matching condition the extent of the solution curve decreases compared to the case of no inhibition. For small values of inhibitory and excitatory width, the two matching conditions intersect, and traveling wave solutions exist. Upon further increasing the inhibitory strength ($g_{ie} = g_{ii} = 0.4$) the matching conditions continue to deform. In

this case, the matching conditions do not intersect, so we conclude that traveling waves exist only in the case of a weak inhibitory effect.

We perform a similar analysis in Fig. 4b but consider a different speed of $c = 400$ μm/ms. In Fig. 4b we observe that the solutions to the excitatory matching conditions (6) have shifted to higher values of excitatory and inhibitory width. The curves of the inhibitory matching conditions (7) have also shifted upwards to larger widths. These observations imply that, in order to support faster waves, the solutions possess larger excitatory and inhibitory wave widths.

To summarize the previous analysis in the case of slow-acting inhibition ($\alpha_i = \alpha_e/10$) we consider in Fig. 4c the existence of waves (i.e., the intersection points) given differents speeds. Again, we observe that faster waves correspond to solutions with larger excitatory and inhibitory wave widths. In particular, we observe an approximate linear relationship such that excitatory wave width increases as wave speed increases. Also, we observe that given a fixed wave speed, a stronger inhibitory effect (orange or red curve in Fig. 4c) produces thinner waves compared to the case of no inhibition. That is, considering a fixed wave speed the effect of inhibition is to reduce wave width. In Fig. 4a–b we note that, in general, as the strength of the inhibitory connectivity increases, the extent of the solutions for the inhibitory waves gets smaller (i.e., the blue curves encompass less area in the figures). This observation suggests that smaller values of inhibitory strength are more likely to produce an intersection of the matching condition curves and therefore support the existence of excitatory and inhibitory waves.

Repeating this analysis for faster inhibitory decay rates ($\alpha_i = \alpha_e$ in Fig. 4d–f, and $\alpha_i = 10\alpha_e$ in Fig. 4g–i), we find qualitatively similar results. In all cases, as the inhibitory strength or the inhibitory decay rate increases, the inhibitory matching conditions yield smaller curves. We note however a significant difference in the wave width determined by faster-acting inhibition. In Fig. 4f we observe that for relatively weak inhibitory effect ($g_{ie} = 0.4$) there are no wave solutions (no red curve). This implies that the inhibitory matching conditions are not present at wave widths consistent with the *in vivo* data (Fig. 4a–b). We also observe that for a slightly weaker inhibitory effect ($g_{ie} = 0.2$) there are three wave solutions for wave speeds greater than c = 300 μm/ms with only one of these solutions lying close to the range of interest. In this case, the strong inhibition has eliminated the existence of physically meaningful solutions. We compare this with the case of strong inhibition ($g_{ie} = 0.4$) acting at a slow time scale ($\alpha_i = \alpha_e/10$); here the inhibitory matching conditions are still present (see the red curve in Fig. 4c). We also note that for faster-acting inhibition ($\alpha_i = \alpha_e$) the intersections of the matching condition curves occur at sligthly smaller widths relative to slower acting inhibition ($\alpha_i = \alpha_e/10$) when inhibition is present. Considering the case of faster-acting inhibition ($\alpha_i = 10\alpha_e$, Fig. 4i) we observe that for relatively weak inhibitory effect (orange and red curves) there exist waves solutions for sufficiently fast waves ($c > 150$ μm/ms in the case of $g_{ie} = 0.2$ and $c > 250$ μm/ms in the case of $g_{ie} = 0.4$) although not all of these solutions are in the range of interest. We also note that for faster waves there exists a small disjoint solution for the excitatory matching condition near the origin. The wave solutions obtained from this curve solution have widths well outside of the range of interest (widths smaller than $w = 1000$ μm) and are not considered further here.

The analysis in Fig. 4 suggests that for slow-acting inhibition ($\alpha_i = \alpha_e/10$), wave solutions exist with the desired features of wave width and wave speed. When inhibition acts on a faster time scale, the model fails to support traveling wave solutions once the inhibitory strength is sufficiently increased. The amount of inhibitory strength necessary to disrupt the existence of waves depends on, among other factors, the speed of the wave and the inhibition timescale. In particular, we note that faster waves exist for larger values of inhibition timescale and strength than slower waves.

2.5 Effect of inhibition on waves of fixed width

Finally, we consider the impact of inhibition on wave solutions to model (2) in which the width of the excitatory wave is fixed. As in the previous sections we analyze solutions to the excitatory and inhibitory matching conditions to identify parameter configurations that support the existence of traveling waves. We examine two different widths of the excitatory wave in Fig. 5 (first column $w = 1000$ μm, and second column $w = 2000$ μm) consistent with the *in vivo* data, and three different inhibitory timescales ($\alpha_i = \alpha_e/10$, $\alpha_i = \alpha_e$ and $\alpha_i = 10\alpha_e$). In the first and second column of Fig. 5 we explore the intersections of the matching condition curves as a function of the inhibitory wave width and excitatory wave speed, and strength of the inhibitory connectivity (g_{ie} and g_{ii}). In the last column of Fig. 5 we summarize these intersections for different inhibitory timescales as the wave width is varied.

We begin by considering the case of slow-acting inhibition (i.e., $\alpha_i = \alpha_e/10$) and a fixed width of $w = 1000$ μm, and examine the effect on the matching conditions of varying the strength of inhibition (g_{ie} and g_{ii}, where $g_{ie} = g_{ii}$). Without inhibition (i.e., $g_{ie} = 0$) the excitatory speed remains constant as the inhibitory width varies. The inhibitory matching condition (blue curve of parabolic shape in Fig. 5a) intersects the excitatory matching condition, and therefore a traveling wave solution exists. Upon increasing the inhibitory strength (to $g_{ie} =$

0.2) we find that the solutions to the excitatory matching conditions exhibit an approximately vertical line near an inhibitory width of 1000 μm. Approaching this width from below, the speed of the excitatory wave rapidly decreases (from above 200 μm/ms to near 0 μm/ms). Beyond 2000 μm solutions to the excitatory matching conditions cease to exist. At these values, the inhibitory wave width exceeds the excitatory wave width. Because the Heaviside functions for both neural populations terminate at the same position (we have fixed $w_{i0} = w_{e0}$), the spatial onset of the inhibitory wave now precedes the spatial onset of the excitatory wave. This increased inhibition prevents the establishment of an excitatory wave. We also note that increasing the inhibitory effect ($g_{ie} = 0.4$) produces intersection points corresponding to faster waves. In Fig. 5c we summarize these results for values of wave widths varying between 1000 to 4000 μm. We observe that, in general, as wave width increases so does the wave speed. Also, if we consider a fixed wave width, increasing the inhibitory strength produces an increase in the wave speed. This implies that for a fixed wave width in the range of interest, a sufficiently strong inhibitory effect (g_{ie}) can potentially produce a wave speed outside the range of interest. We also note that solutions to the matching conditions still exist for all widths greater than 1000 μm. However, the corresponding wave speeds are small (less than 50 μm/ms) and these solutions do not produce traveling wave solutions of the model. The previous results show that, as the strength of inhibition increases (i.e., g_{ie} increases from 0) or the width of the inhibitory wave increases, the speed of the excitatory wave also increases. We might think of this physically as the excitatory wave "outrunning" the local effects of inhibition and thus continuing to propagate.

We conclude this discussion of Fig. 5a, b, c with the following summary. First, the excitatory matching conditions provide a maximum limit on the inhibitory width corresponding to the fixed width chosen for the excitatory wave. Second, up to this maximum limit the speed of the excitatory wave solution increases as the inhibitory wave width increases. In the case of active inhibition ($g_{ie} > 0$) the maximum speed of the excitatory wave solution occurs near the maximum inhibitory width. Third, the speed of the traveling wave solutions increases as the strength of inhibition increases.

Repeating this analysis for faster inhibitory decay rates ($\alpha_i = \alpha_e$ in Fig. 5d–f, and $\alpha_i = 10\alpha_e$ in Fig. 5g–i) we find qualitatively similar results. For non-zero inhibition ($g_{ie} > 0$), the excitatory matching conditions produce solution curves in which the speed of the excitatory wave increases with increasing inhibitory wave width, up to the limit at which the excitatory and inhibitory wave widths are equal. The inhibitory matching conditions maintain a parabolic shape that shifts upwards as the strength of inhibition increases. We note, however, a quantitave change in the existence of waves. In the case of slow-acting inhibition (Fig. 5c) we observe a broader existence of waves for stronger inhibitory effects (up to 3000 μm for $g_{ie} = 0.4$ and up to near 4000 μm for $g_{ie} = 0.2$) compared to inhibition acting at the same timescale as excitation (Fig. 5f, wave width of up to 2000 μm for $g_{ie} = 0.4$ and near 3000 μm for $g_{ie} = 0.2$) and faster-acting inhibition (Fig. 5i, wave width of up to 2500 μm for $g_{ie} = 0.4$ and near 3500 μm for $g_{ie} = 0.2$.) For wider waves ($w = 4000$ μm) and faster inhibitory decay rates ($\alpha_i >= \alpha_e$) traveling waves exist only in the case of no inhibition. Therefore, we conclude that, in general, traveling wave solutions in the physical range of interest exist for model (2) for inhibition at relatively weak inhibitory strengths. Also, we observe a broader existence of waves for relatively stronger inhibitory effects in the case of slow-acting inhibition.

2.6 Summary of the effects of inhibition

We now summarize the effects of inhibition on the existence of traveling wave solutions to model (2). To do so, we consider conditions in which the traveling waves exist and observe the effect on these conditions for different decay rates (α_i) and strengths (g_{ie}) of the inhibitory population. In this way, instead of analyzing the existence of waves determined by the matching conditions given by fixed inhibitory strengths ($g_{ie} = 0.2$ and $g_{ie} = 0.4$) as shown in Figs. 4 and 5 we here examine the existence of traveling waves for different inhibitory strengths (g_{ie} up to 1). In doing so, we fix the wave speed (first row of Fig. 6) or excitatory wave width (second row of Fig. 6) and vary g_{ie} and α_i.

In Fig. 6a we consider a wave speed of $c = 200$ μm/ms and analyze the effect of increasing the inhibitory effect for different inhibition timescales. In the case of slow-acting inhibition, i.e., $\alpha_i = \alpha_e/10$ (red curve in Fig. 6a), we observe that traveling waves exist for excitatory wave widths less than 1200 μm. As the strength of inhibition increases, the maximum excitatory width decreases, and when the inhibition strength is large enough the traveling wave solutions cease to exist. We note that two wave solutions of different widths exist for values of g_{ie} between 0 and 0.4. As the decay rate increases, traveling wave solutions exist only for smaller values of inhibitory strength (blue and green curves in Fig. 6a). For a larger value of wave speed ($c = 400$ μm/ms, Fig. 6b) traveling wave solutions exist for a larger interval of inhibitory strength. In the case of slow-acting inhibition $\alpha_i = \alpha_e/10$ traveling waves exist for excitatory widths of less than 2500 μm and for inhibitory strengths greater than $g_{ie} = 1$. In this case, four wave solutions exist with different widths (i.e., red curves in Fig. 6b). As the timescale of inhibition increases, the traveling wave solutions become restricted

to smaller values of inhibitory strength. In the case of inhibition acting at the same timescale as excitation ($\alpha_i = \alpha_e$) wave solutions exist up to $g_{ie} = 0.25$ and in the case of faster-acting inhibition ($\alpha_i = 10\alpha_e$) wave solutions exist up to $g_{ie} = 0.6$. We conclude that, in general, as the strength of inhibition increases the corresponding excitatory wave width decreases until it either ceases to exist or leaves the range of physical interest. In the case of slow-acting inhibition traveling wave solutions exist even with a relatively strong inhibitory effect. We show here that the amount of inhibition that can be sustained depends on the wave speed and inhibitory decay rate.

In Fig. 6c–d we perform a similar analysis but now vary the excitatory wave width. For an excitatory width of $w = 1000$ μm (Fig. 6c) and a slow-acting inhibition ($\alpha_i = \alpha_e/10$) we find traveling waves with a speed of more than 150 μm/ms. As in the previous panels, the two red curves denote the existence of two traveling wave solutions in the case of slow-acting inhibition. We note that there also exists a very slow wave solution (with speeds of less than 10 μm/ms). We do not consider these solutions as the speeds are too slow to match the *in vivo* data. As the strength of inhibition increases to $g_{ie} = 1$, the speed of the waves increases and lies in the range of physical interest. For faster-acting inhibition we obtain similar results although the wave speeds exit the range of physical interest when the strength of inhibition is large enough, greater than $g_{ie} = 0.6$, although one wave solution stays in the range of interest for fast-acting inhibition (blue curve in Fig. 6c). Increased excitatory wave widths support similar qualitative results ($w = 3000$ μm in Fig. 6d). The wave speeds continue to increase with the strength of inhibition, but do so more rapidly for wider excitatory waves.

We conclude from these results that it is more likely to obtain traveling wave solutions in the physically meaningful range of speeds and widths when the inhibition is slow and weak. We show in Fig. 6a–d that for slow-acting inhibition ($\alpha_i = \alpha_e/10$) it is possible to obtain traveling wave solutions for a broad range of inhibitory strengths. The degree of inhibitory strength that supports traveling waves is related to features of the wave, including the speed and width of the excitatory wave. Once the inhibitory population acts on a faster time scale, increasing the strength of the inhibitory population limits the existence of traveling wave solutions with the desired properties.

3 Simulations

In this section we corroborate the results obtained above through analysis of the matching conditions by computing numerical simulations of model (2). In doing so, we replace the Heaviside function in Eq. (2) with a sigmoid function for the excitatory and inhibitory populations $\left(S_j(x) = \frac{1}{1+e^{a_j(k_j - x)}}\right)$ where $j = \{e, i\}$. We choose to do so because a continuous sigmoid is more biophysically realistic than a discontinuous Heaviside function. For illustration purposes we fix the value of $a_e = a_i = 50$, and thus we consider a relatively steep change of the sigmoid near the activity threshold. The MATLAB code to perform these numerical simulations is available for reuse and modification at https://github.com/Mark-Kramer/Effect-of-inhibition-on-traveling-waves.

We now perform numerical simulations to validate the analytic results. To do so, we obtain parameter ranges for which we have shown traveling waves exist and compute numerical simulations of the model based on these parameters (see Fig. 7). The simulations in all figures have the fixed parameters: $\beta = 2.5$, $\alpha_e = 1$, $\delta = 0.1$, $\sigma_{ee} = \sigma_{ei} = 600$ μm and $\sigma_{ie} = \sigma_{ii} = 100$ μm. In each subfigure we begin with an initial excitatory perturbation (at position 0 to 70 μm of duration 3 ms) and simulate traveling waves with wave speed $c \approx 500$ μm/ms and different wave widths (varying between $w \approx 1600$ μm and $w \approx 3000$ μm). The wave width is determined by the matching conditions and the remaining fixed parameters c, α_i, k_e, g_{ie}. In the case of no inhibition (i.e., $g_{ie} = 0$) we obtain from the matching conditions (6)–(7) the existence of a wave with width $w \approx 2800$ μm and speed $c \approx 500$ μm/ms for $k_e = 0.23$. In the numerical simulations (Fig. 7a), we obtain a traveling wave with wave speed $c \approx 515$ μm/ms and wave width $w \approx 3200$ μm using a synaptic threshold of $k_e = 0.105$. In the case of slow-acting inhibition ($\alpha_i = 0.1$) and inhibitory strength of $g_{ie} = 0.2$ we obtain from the matching conditions (6)–(7) the existence of a wave with width $w \approx 2500$ μm and speed $c \approx 500$ μm/ms for $k_e = 0.17$. In the numerical simulations (Fig. 7b) we obtain a traveling wave with wave speed $c \approx 500$ μm/ms and wave width $w \approx 2920$ μm using a synaptic threshold of $k_e = 0.1$. Then, increasing the inhibitory strength to $g_{ie} = 0.4$ we obtain from the matching conditions (6)–(7) the existence of a wave with width $w \approx 2100$ μm and speed $c \approx 500$ μm/ms for $k_e = 0.17$. In the numerical simulations (Fig. 7c), we obtain a traveling wave with wave speed $c \approx 510$ μm/ms and wave width $w \approx 2800$ μm using a synaptic threshold of $k_e = 0.1$. In the case of faster inhibition ($\alpha_i = 1$) and inhibitory strength of $g_{ie} = 0.2$ we obtain from the matching conditions (6)–(7) the existence of a wave with width $w \approx 1600$ μm and speed $c \approx 500$ μm/ms for $k_e = 0.18$. Then, in the numerical simulations (Fig. 7d), we find that a traveling wave appears briefly, with wave speed $c \approx 480$ μm/ms and wave width $w \approx 2200$ μm using a synaptic threshold of $k_e = 0.064$. However, this wave fails to propagate after 5 ms. We thus conclude that, when inhibition is absent (Fig. 7a), slow and

weak (Fig. 7b), or slow and strong (Fig. 7c), then traveling waves persist. However, when the inhibition is fast and weak, traveling waves cease to propagate (Fig. 7d). These numerical simulations are consistent with the analytic results: traveling waves exist when inhibition is slow and weak.

4 Conclusions

We showed in González-Ramírez et al. (2015) that the neural field model (1) is capable of reproducing important features observed in clinical traveling wave data approaching seizure termination, in particular the wave speed, width and features of the reverberation of activity. However, this model assumed that inhibitory activity was not present. Here, we have added the effect of an inhibitory population to create the model (2). In this model we again found parameter ranges that support wave propagation consistent with human clinical data. More specifically, we found that inhibition acting on a slow timescale (i.e., on a timescale a factor of 10 times slower than the timescale of excitation) permits the existence of traveling waves. However, if the inhibition acts on a faster timescale or we increase the strength of inhibition, traveling waves cease to exist. In addition, we showed that in this model the speed of the traveling wave solutions increase with the strength of inhibition. This suggests -in the context of model (2)—a relationship between wave speed (an easily observed quantity from *in vivo* data) and an unobserved biophysical mechanisms (the strength of inhibition). Detailed models of single neuron activity present many other biological features that could impact traveling wave dynamics (Compte et al. 2003; Muller and Destexhe 2012; Destexhe et al. 1996); understanding how to incorporate these mechanisms into neural population models, and the impact on traveling wave dynamics during seizure, remains an open research challenge. We conclude that model (2) supports the wave phenomena observed *in vivo* when inhibition acts on a slow timescale or its effect is weak. We postulate that stronger or faster inhibition may serve as a restorative healthy mechanism that disrupts the pathological traveling waves observed preceding seizure termination.

Acknowledgements MAK acknowledges support from NSF DMS 1451384 and NIH NINDS R01NS072023.

Compliance with Ethical Standards

Conflict of interest The authors declare that they have no conflict of interest.

References

Amari, S. (1977). Dynamics of pattern formation in lateral inhibition type neural fields. *Biological Cybernetics*, *27*, 77–87.

Bojak, I., & Liley, D.T.J. (2005). Modeling the effects of anesthesia on the electroencephalogram. *Physical Review E*, *71*, 041902.

Bojak, I., Liley, D.T.J., Cadusch, P.J., Cheng, K. (2004). Electrorhythmogenesis and anaesthesia in a physiological mean field theory. *Neurocomputing*, *58–60*, 1197–202.

Braitenberg, V., & Schuz, A. (1998). *Cortex: statistics and geometry of neuronal connectivity*. Berlin: Springer.

Bressloff, P.C. (2001). Traveling fronts and wave propagation failure in an inhomogeneous neural network. *Physica D*, *155*, 83–100.

Bressloff, P.C. (2012). Spatiotemporal dynamics of continuum neural fields. *Journal of Physics A: Mathematical and Theoretical*, *45*, 033001.

Bressloff, P.C. (2014). *Waves in neural media, Lecture notes on mathematical modelling in the life sciences*. Berlin: Springer.

Bressloff, P.C., Cowan, J.D., Golubitsky, M., Thomas, P.J., Wiener, M. (2001). Geometric visual hallucinations, Euclidean symmetry and the functional architecture of striate cortex. *Philosophical Transactions of the Royal Society B*, *356*, 299–330.

Bressloff, P.C., & Webber, M.A. (2011). Neural field model of binocular rivalry waves. *Journal of Computational Neuroscience*. https://doi.org/10.1007/s10827-011-0351-y.

Chervin, R.D., Pierce, P.A., Connors, B.W. (1988). Periodicity and directionality in the propagation of epileptiform discharges across neocortex. *Journal of Neurophysiology*, *60*, 1695–1713. PMID: 3143812.

Compte, A., Sanchez-Vives, M.V., McCormick, D.A., Wang, X.J. (2003). Cellular and network mechanisms of slow oscillatory activity (<1 Hz) and wave propagations in a cortical network model. *Journal of Neurophysiology*, *89*(5), 2707–2725.

Coombes, S. (2005). Waves, bumps, and patterns in neural field theories. *Biological Cybernetics*, *93*, 91–108.

Coombes, S., beim Graben, P., Potthast, R., Wright, J. (2014). *Neural fields: theory and applications*. Berlin: Springer.

Destexhe, A., Bal, T., McCormick, D.A., Sejnowski, T.J. (1996). Ionic mechanisms underlying synchronized oscillations and propagating waves in a model of ferret thalamic slices. *Journal of Neurophysiology*, *76*(3), 2049–2070.

Ermentrout, G.B. (1998). Neural Networks as spatio-temporal pattern-forming systems. *Reports on Progress in Physics*, *61*, 353–430.

Ermentrout, G.B., & Cowan, J. (1979). A mathematical theory of visual hallucination patterns. *Biological Cybernetics*, *34*, 137–50.

Ermentrout, G.B., & Terman, D.H. (2010). *Mathematical foundations of neuroscience*. Berlin: Springer.

Foster, B.L., Bojak, I., Liley, D.T.J. (2011). Understanding the effects of anesthetic agents on the eeg through neural field theory. In *Conference of the IEEE engineering in medicine and biology society 4709-12, 652*, https://doi.org/10.1109/IEMBS.2011.6091166.

Fuster, J.M., & Alexander, G. (1971). Neuron activity related to short-term memory. *Science*, *173*, 652.

Golomb, D., & Amitai, Y. (1997). Propagating neuronal discharges in neocortical slices: computational and experimental study. *Journal of Neurophysiology*, *78*, 1199–1211.

González-Ramírez, L.R., Ahmed, O., Cash, S.S., Wayne, C.E., Kramer, M.A. (2015). A biologically constrained, mathematical model of cortical wave propagation preceding seizure termination. *PLoS Computational Biology*, *11*(2), e1004065.

Huang, X., Troy, W.C., Yang, Q., Ma, H., Laing, C., Schiff, S., Wu, J.Y. (2004). Spiral waves in disinhibited mammalian cortex. *The Journal of Neuroscience*, *24*, 9897–9902.

Jirsa, V.K., & Haken, H. (1996). Field theory of electromagnetic brain activity. *Physical Review Letters*, *77*, 960–3.

Kilpatrick, Z.P., Folias, S.E., Bressloff, P.C. (2008). Traveling pulses and wave propagation failure in inhomogeneous neural media. *SIAM Journal on Applied Dynamical Systems*, *7*, 161–185.

Kramer, M.A., Kirsch, H.E., Szeri, A.J. (2005). Pathological pattern formation and cortical propagation of epileptic seizures. *Journal of the Royal Society, Interface*, *2*, 113–127.

Lee, U., Kim, S., Jung, K. (2006). Classification of epilepsy types through global network analysis of scalp electroencephalograms. *Physical Review E*, *73*, 041920.

Liley, D.T.J., & Bojak, I. (2005). Understanding the transition to seizure by modeling the epileptiform activity of general anesthetic agents. *Journal of Clinical Neurophysiology*, *22*, 5.

Liley, D.T.J., Cadusch, P.J., Dafilis, M.P. (2002). A spatially continuous mean field theory of electrocortical activity. *Network*, *13*, 67–113.

Markram, H., Toledo-Rodríguez, M., Wang, Y., Gupta, A., Silberberg, G., Wu, C. (2004). Interneurons of the neocortical inhibitory system. *Nature Reviews Neuroscience*, *5*(10), 793–807.

Milton, J., & Jung, P. (2003). *Epilepsy as a dynamic disease*. Berlin: Springer.

Muller, L., & Destexhe, A. (2012). Propagating waves in thalamus, cortex and the thalamocortical system: experiments and models. *Journal of Physiology*, *106*(5–6), 222—238. https://doi.org/10.1016/j.jphysparis.2012.06.005.

Nunez, P.I. (1995). *Neocortical dynamics and human EEG rhythms*, (p. 708). New York: Oxford University Press.

Pinto, D.J., & Ermentrout, G.B. (2001). Spatially structured activity in synaptically coupled neuronal networks: II. Lateral inhibition and standing pulses. *SIAM Journal on Applied Mathematics*, *62*(1), 226–243.

Pinto, D.J., Brumberg, J.C., Simons, D.J., Ermentrout, G.B. (1996). A quantitative population model of whisker barrels: re-examining the Wilson-Cowan equations. *Journal of Computational Neuroscience*, *3*, 247–264.

Pinto, D.J., Patrick, S.L., Huang, W.C., Connors, B.W. (2005). Initiation, propagation, and termination of epileptiform activity in rodent neocortex *in vitro* involve distinct mechanisms. *The Journal of Neuroscience*, *25*(36), 8131/81-40, 247–264.

Robinson, P.A., Loxley, P.N., O'Connor, S.C., Rennie, C.J. (2001). Modal analysis of corticothalamic dynamics, electroencephalographic spectra and evoked potentials. *Physical Review E*, *63*, 041909-13.

Shusterman, V., & Troy, W.C. (2008). From baseline to epileptiform activity: a path to synchronized rhythmicity in large-scale neural networks. *Physical Review E*, *77*, 061911.

Smith, E.H., Liou, J., Davis, T.S., Merricks, E.M., Kellis, S.S., Weiss, S.A., et al (2016). The ictal wavefront is the spatiotemporal source of discharges during spontaneous human seizures. *Nature Communications*, *7*, 1–12.

Spencer, J.P., & Schoner, G. (2006). An embodied approach to cognitive systems: a dynamic neural field theory of spatial working memory. In *Proceedings of the 28th annual conference of the cognitive science society* (pp. 2180–2185).

Steyn-Ross, M.L., Steyn-Ross, D.A., Sleigh, J.W., Liley, D.T.J. (1999). Theoretical EEG stationary spectrum for a white-noise-driven cortex: evidence for a general anesthetic-induced phase transition. *Physical Review E*, *60*, 7299–311.

Toubol, J., Wendling, F., Chauvel, P., Faugeras, O. (2013). Neural mass activity, bifurcations and epilepsy. *Neural Computation*, *23*(12), 3232–3286.

Traub, R., Contreras, D., Cunningham, M., Murray, H., LeBeau, F., Roopun, A., et al. (2005). Single-column thalamocortical network model exhibiting gamma oscillations, sleep spindles, and epileptogenic bursts. *Journal of Neurophysiology*, *93*, 2194–2232.

Wadman, W.J., & Gutnick, M.J. (1993). Non-uniform propagation of epileptiform discharge in brain slices of rat neocortex. *Neuroscience*, *52*, 255–262. https://doi.org/10.1016/0306-4522(93)90154-8PMID:8450945.

Wagner, F.B., Eskandar, E.N., Crosgrove, G.R., Madsen, J.R., et al (2015). Microscale spatiotemporal dynamics during neocortical propagation of human focal seizures. *Neuroimage*, *122*, 114–30.

Wilson, H.R., & Cowan, J.D. (1973). A mathematical theory of the functional dynamics of cortical and thalamic nervous tissue. *Cybernetik*, *13*, 55–80.

Wu, J.Y., Guan, L., Bai, L., Yang, Q. (2001). Spatiotemporal properties of an evoked population activity in rat sensory cortical slices. *Journal of Neurophysiology*, *86*, 2461–74. PMID: 11698535.

Xiao, Y., Huang, X.Y., Van Wert, S., Barreto, E., Wu, J.Y., Gluckman, B.J., Schiff, S.J. (2012). The role of inhibition in oscillatory wave dynamics in the cortex. *European Journal of Neuroscience*, *36*, 2201–2212.